JOURNAL OF AIRCRAFT
Vol. 39, No. 4, July–August 2002

Hover Test of Mach-Scale Active Twist Rotor Using Piezo-Bending–Torsion Actuators

Andreas P. F. Bernhard* and Inderjit Chopra†
University of Maryland, College Park, Maryland 20742

The active twist rotor investigated in this research is a derivative of the previously developed smart-active-blade-tip (SABT) rotor. On the SABT rotor, the blade tips are independently pitched, with respect to the main blade. A novel piezo-induced bending–torsion coupled actuator beam, located spanwise in the hollow midcell of the main rotor blade, is used to actuate the blade tip. When the blade tip is locked to the main blade, the actuator beam twists the entire blade. A Mach scale rotor with a 1.542 m diameter was hover tested, open loop, to evaluate the control authority for vibration reduction. A nonrotating tip-twist amplitude of 0.78 deg was achieved (below resonance, 150 V rms). Analysis indicates that no significant twist actuation degradation is expected at full rotor speed. In 2000-rpm hover (tip Mach 0.47), at 8-deg collective, and for a single blade actuation of 150 V rms at 1, 2, and 3 per revolution, respectively, the measured oscillatory thrust coefficients are 1.4×10^{-3}, 0.55×10^{-3}, and 0.7×10^{-3}. The corresponding finite element model estimated blade twist amplitudes are 0.8, 1.0, and 1.9 deg. Good correlation of the predicted and measured rotor thrust was achieved up to 3 per revolution. The hover test demonstrates the potential of the active twist rotor system using an internal actuation beam and warrants further research for a dedicated next-generation model-scale design and full-scale feasibility study.

Introduction

HIGH vibration levels limit helicopter performance and reduce the structural life of components. This imposes an expensive maintenance burden and raises reliability concerns. The high vibration (in conjunction with high noise levels) also leads to pilot fatigue and a poor ride quality. Significant research is presently dedicated toward realizing the goal of jet-smooth and quiet rotary-wing flight, to improve the cost effectiveness and to achieve wider community acceptance of rotorcraft.

Traditionally, passive vibration absorbers and isolators are used to tackle the vibration problem. However, they incur a large weight penalty and exhibit poor off-design performance, especially considering the wide flight envelope of the helicopter. To improve vibration-reduction performance across the flight envelope, active control strategies are being considered. Recent developments in smart materials and control strategies have opened the domain of smart vibration-reduction techniques.[1–6] These feature adaptive control strategies employing distributed sensors and actuators that enable performance and ride-quality improvement over a large variety of flight conditions.

When active control strategies are used in conjunction with on-blade actuation, it is possible to attack vibration and noise directly at its source, in the rotating frame. Numerous active control systems have been proposed and to some extent developed and tested.[1] The two most common rotating-frame, active-rotor concepts are the trailing-edge flap rotor[7–23] and the active twist rotor.[24–33] Discrete trailing-edge flaps offer advantages in terms of blade modularity, existing-blade retrofits, and multiflap control flexibility. In contrast, direct internal twist actuation is aerodynamically cleaner, eliminating the drag penalty associated with discrete flaps. Recently, there has also been interest in next-generation active-rotor technology: swashplateless rotor control.[34,35]

The first active twist rotor using direct twist actuation was developed by Chen and Chopra[24,25] and Chen[26] at the University of Maryland. The rotor blade incorporated discrete dual-layer monolithic piezopatch elements embedded at +45 deg under the upper skin and −45 deg under the lower skin of the rotor blade. A 1.83-m-(6-ft) diameter Froude-scale active twist rotor was tested in hover and in the wind tunnel. The tip Mach number of the reduced speed rotor was 0.28. Blade-tip-twist amplitudes of ±0.5 deg were achieved (excitation level 150 V rms) at advance ratios up to 0.33. The open-loop wind-tunnel tests demonstrated that, despite the low blade-tip-twist amplitudes, it was possible to appreciably alter the rotor hub loads.

The precursor to the preceding active twist rotor was the work on directionally attached piezoceramics.[36,37] Another implementation of the directionally attached piezotechnology was used in developing a small-scale remote-piloted helicopter with active twist flexbeams.[38] The active twist flexbeams pitched servocontrol paddles and eliminated the swashplate. This resulted in a 40% control system weight reduction and an estimated 26% reduction in parasite drag. Flight tests demonstrated functional controllability of the swashplateless helicopter.

With the emergence of piezofiber technology, the active twist concept was dramatically improved. With this technology, it is possible to create an active piezoply within a composite laminate, enabling the smart structures vision of active elasticity. The continuous piezoply is structurally more effective than the embedded discrete monolithic piezoelements used in the preceding two active twist rotor concepts. The primary challenges in piezofiber technology are achieving uniformity of material properties and actuation characteristics, developing robust interdigitated electrode technology, and reducing fabrication costs. The main disadvantage of the piezofiber technology is the requirement for very high voltages, on the order off 1–2 kV. The piezofiber concept was originally developed by Bent and Hagood,[39] Rogers and Hagood,[40] and Rogers et al.[41] and has subsequently been commercialized.[42] For the active twist blade application, the piezofibers are used to form active plies within the overall spar laminate. The piezoplies are oriented at +45 and −45 deg to achieve torsional actuation. Derham and Hagood[43] undertook a preliminary design and cost analysis for active twist blades for The Boeing Company CH-47 Chinook. After the potential viability of the concept was demonstrated, a cooperative Boeing

Received 26 February 2001; revision received 12 December 2001; accepted for publication 28 March 2002.

*Gustave J. Hokenson Fellow, Alfred Gessow Rotorcraft Center; currently, Dynamicist, Sikorsky Aircraft Corporation, M/S S317A, 6900 Main Street, Stratford CT 06615; abernhard@sikorsky.com.

†Alfred Gessow Professor and Director, Alfred Gessow Rotorcraft Center, Department of Aerospace Engineering; chopra@eng.umd.edu. AIAA Fellow.

Company/Massachusetts Institute of Technology program was launched to design, fabricate, and test one-sixth-scale rotor blades.[28,29,44] A two-bladed Mach scale rotor with 3.079 m diameter and 136.9 mm chord was tested with one active blade and one passive balance blade. The design rotor speed was 1336 rpm. The piezofibers were only included in the upper and lower surface of the D-spar laminate, extending over 35.6% of the chord, and were not included in the fairing (primarily because of mass-balancing considerations). The Mach-scale, open-loop hover tests demonstrated the potential to alter the blade flap bending and torsional loads. During the test program, numerous problems were encountered with electrical failure of the active fiber packs. A tip twist of ± 0.4 deg was achieved, with a low-frequency excitation of ± 1 kV, at full rotor speed (tip Mach 0.63) and 8 deg collective. A corresponding low-frequency excitation oscillatory thrust coefficient of 1.3×10^{-4} was measured (one blade active). The blade torsional frequency was 4.4 per revolution. The mass penalty of the active twist blade, compared to the baseline blades, was approximately 16%. To differentiate active blade twist generated by servoflaps and embedded induced strain actuation, the latter concept has been referred to as integral twist actuation in the literature.

Based on the success of the proof-of-concept demonstration, a second-generation active twist Mach-scale Chinook CH-47 model rotor was developed and fabricated by The Boeing Company.[32] The rotor incorporated advanced airfoils and planform and improved piezofiber packs and electrical harnessing. In hover, a tip twist of ± 1.4 deg was measured, and an oscillatory thrust authority over 10% was demonstrated. A key aspect highlighted in the design analysis was that the rotor design may be driven by worst-case erroneous blade actuation resulting in increased blade loads.

Following the proof-of-concept work by Rodgers and Hagood,[44] NASA Langley Research Center also developed an active twist rotor.[30,31,45] A one-sixth-scale active twist blade with a symmetric NACA 0012 profile was fabricated and tested in the Transsonic Dynamics Tunnel wind tunnel. The tests were conducted in a heavy gas medium (R134a) to achieve simultaneous Froude and Mach scaling. The rotor blades have a diameter of 2.794 m and a chord of 107.7 mm. Two active plies were included in the upper and lower D-spar layup and extend from 4.5 to 44.3% chord. With improvements in the fabrication of the active fiber packs and the interdigitated electrodes, the failure rate of the fiber packs was dramatically reduced, compared to the proof-of-concept rotor developed by Rodgers and Hagood. Wind-tunel test results demonstrated blade-tip-twist amplitudes of ± 1.1 to 1.4 deg at excitation frequencies of 3–5 per revolution. With further improvements in the fabrication and integration of the active fiber packs, the twist performance can be increased to reach the tip-twist target of ± 2 deg for complete vibration control. Rotating and fixed system loads were significantly altered by the twist actuation and effective open-loop vibration reduction was demonstrated. Closed-loop wind-tunnel tests are planned for 2002. In parallel with the experimental active twist research, extensive work has been done on the detailed modeling of active fiber composites and active twist blades,[46–48] in addition to further characterization of piezofiber material properties.[49]

An interesting development in the field of piezofiber technology is macrofiber composite (MFC) actuators,[50] developed by NASA Langley Research Center/U.S. Army Research Laboratory. These actuators consist of "fibers" cut from a monolithic piezoceramic sheet that are subsequently embedded in an epoxy matrix with interdigitated electrodes. MFC actuator technology promises improvements in the uniformity of actuator properties and enhanced actuator performance compared to extruded piezofibers. MFC fiber packs may be attractive for next-generation active twist rotor designs.

The preceding active twist concepts are based on discrete or continuous induced-strain actuators embedded within the blade spar/skin and, hence, are an integral part of the primary blade structure. An alternative to integral blade twist actuation is to use an internal actuator beam (within the blade spar) to twist the rotor blade. The advantage of this is that the primary blade structure and actuator are separated. Hence, actuator failure does not require replacing an entire rotor blade. For example, DLR, German Aerospace Research Center, has performed some work on closed-cell warping–torsion coupling of the spar and extension–torsion coupling of the blade skin for blade twist actuation,[33,51,52] using discrete actuators within the blade.

For the present investigation, a piezo-induced bending–torsion coupled beam, mounted within the blade spar, is proposed as solid-state torsion actuator to twist the rotor blade. The actuator beam was in fact developed for a smart rotor incorporating active pitching blade tips for vibration control. The design, development, and Mach-scale hover testing of the active tip rotor was reported in Refs. 53–55. When the blade tips are locked to the main blade, the spanwise actuator beam within the rotor blade will tend to twist the entire blade. The focus of this paper is on the Mach-scale hover testing of the rotor in active twist configuration.

Actuation Concept

A schematic of the rotor blade with a smart active blade tip (SABT) is shown in Fig. 1. The blade tips are locked down for the SABT active twist (ATW) configuration SABTatw. In this configuration the actuator beam functions as an active torsion spring in parallel with the blade. Induced-strain actuation of the beam generates blade twist.

The rotor blades are actuated by a unique piezo-induced, bending–torsion coupled composite actuator beam that is located spanwise within the hollow midcell of the three cell blade cross section. Figures 2 and 3 show the schematics of this structural actuator. The main components of the bending-torsion actuator are 1) composite beam with structural bending–torsion coupling, 2) reversed

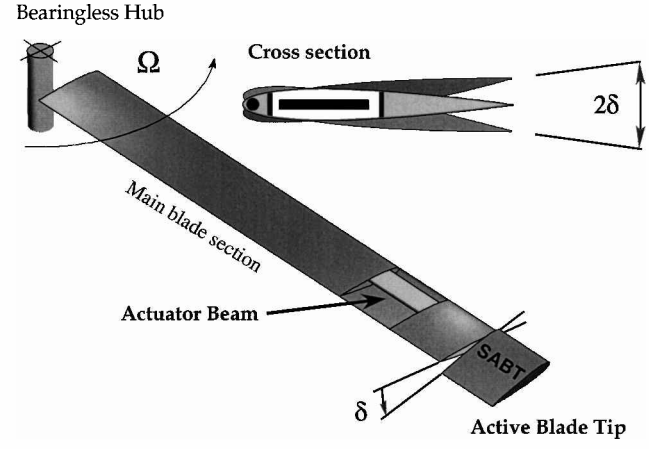

Fig. 1 SABT concept schematic; in active twist configuration blade tips are locked to main blade.

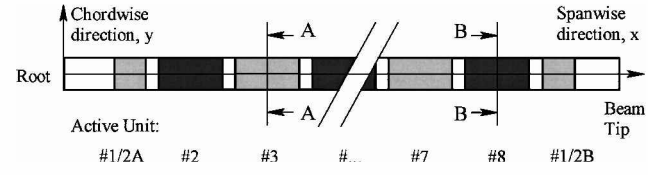

Top view of actuator beam

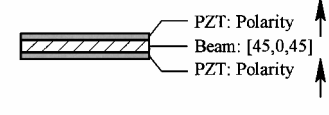

Section A–A

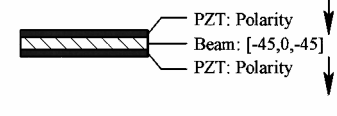

Section B–B

Fig. 2 Schematic of the piezo-induced, bending–torsion coupled actuator beam.

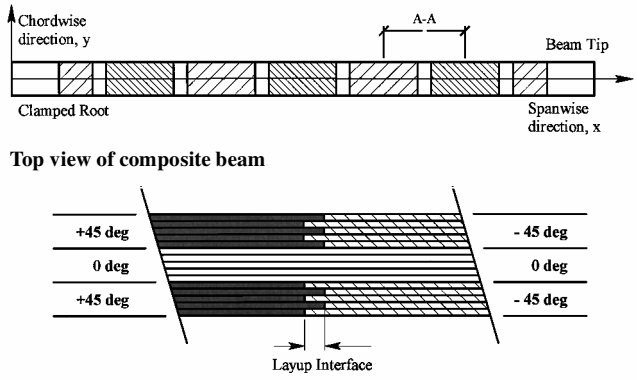

Fig. 3 Composite bending–torsion beam: layup detail.

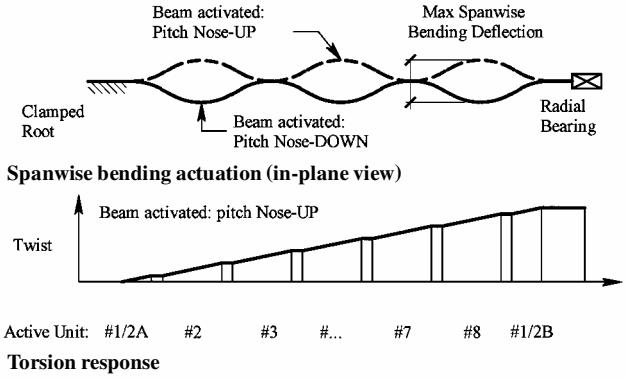

Fig. 4 Schematic of actuator beam mechanics.

bending–torsion coupling for each successive spanwise beam segment, and 3) surface bonded induced-strain actuators with reversed polarity directions over each successive beam segment.

Figure 3 shows a cross section through the layup interface between two segments. The composite beam is not uniform along its length and essentially consists of individual segments in the spanwise direction. For each of these segments, the ply layup in the thickness direction is midplane symmetric and, hence, exhibits a bending–torsion (and extension–shear) coupling. The alternating spanwise +45- and −45-deg segments result in a reversal of the bending–torsion coupling for each successive element. For structural integrity, a set of continuous 0-deg plies runs through the middle of the beam (which does not significantly reduce the bending–torsion coupling). Each beam segment with surface bonded PZT pairs essentially forms a structurally coupled, two-dimensional bimorph unit. These bimorph units effectively twist as they bend. Because of the flip-flopping bimorph excitation, the beam deflects in a spanwise sinusoidal bending wave, and as a result of the alternating bending–torsion coupling, the induced twist is additive over the length of the beam. This is demonstrated in Fig. 4, for both a nose-up and a nose-down activation. The outboard end of the actuator, thus, sees the solid-state actuator as a pure torsional actuator. For further details on the actuator beam see Refs. 53 and 55–57.

Mach-Scale Rotor

The original concept validation of the active blade tip was performed on a reduced tip speed (tip Mach 0.26) active blade-tip rotor on the Boeing ITR bearingless hub, documented in Refs. 53 and 58. The second design iteration transitioned the design to a Mach-scale rotor on a Bell-412 hub. The primary design targets were a twist actuation of ±2 deg and a mass penalty of 20%. Tables 1 and 2 summarize the design configuration for the Mach-scale active blade tip/active twist rotor. Unless specified otherwise, all of the data is based on measurements. For detailed information on design objectives and actuator trade study, see Ref. 55.

Table 1 Mach-scale rotor specifications

Parameter	Value
Nominal physical scale factor	0.125
Number of blades	4
Hub type	Bell-412
Operating speed, rpm	2000
Diameter, m	1.524
Chord, mm	76.2
Tip Mach number	0.47
Lock number	2.55
Tip Reynolds number	0.8325×10^6
Airfoil	NACA 0012
Solidity	0.1273
Precone, deg	2.5
Blade twist, deg	0
Blade sweep (aft), deg	0
Quarter chord torque offset (foward), mm	3.33
Aerodynamic root cutout, %	20.9
Blade mass, g	310
Blade reference mass m_0, kg/m	0.4415
Main blade EI_{flap}, Nm^2	15.40
Main blade EI_{lag}, Nm^2	630
Main blade GJ, Nm^2	7.21
Flap frequency (2000 rpm), per revolution	1.03
Lag frequency (2000 rpm), per revolution	0.944
Torsion frequency (2000 rpm), per revolution	3.79
Thrust, $\theta_0 = 8$ deg, N	315[a]
C_T, $\theta_0 = 8$ deg	5.523×10^{-3}
C_T/σ, $\theta_0 = 8$ deg	0.0434
Rotor power,[b] $\theta_0 = 8$ deg, kW	4.365
C_P,[b] $\theta_0 = 8$ deg	0.480×10^{-3}

[a]Measured (calculated 382 N). [b]Calculated.

Table 2 Active blade-tip and actuator specifications

Parameter	Value
Blade-tip span, %R	10
Blade-tip mass,[a] g	27
Actuator beam mass, g	105.5
Actuation system mass,[b] g	148
Actuator beam length, mm	540
Actuator beam width, mm	25.4
Graphite–epoxy	IM7-8552
Graphite thickness, mm	2.67
Graphite layup	$[45_5,0_5,45_5]$
Active unit interface, mm	6.35
Piezoceramic material	PZT-5H
Piezo thickness, mm	0.254
Number of active units	8
Nominal capacitance,[c] μF	2.1
Current, 150 V peak, 5 per revolution, A	0.8–1.0
Power factor, 150 V rms, 5 per revolution	0.22
Actuator beam effective GJ, Nm^2	4.509
0-rpm natural frequency, Hz	126
0-rpm damping, %	1.4–1.7
Nonrotating tip twist,[d] deg	±0.8
Rotating tip twist,[e] deg	±1.0–±2.2
Piezo actuation, 100 V rms, microstrain	220
Piezo actuation, 150 V rms,[f] microstrain	330

[a]Includes shaft and beam adapter.
[b]Includes shaft assembly and support structures.
[c]0 rpm, 0 V rms.
[d]150 V rms (330 microstrain), 15 Hz, 0 rpm.
[e]150 V rms (330 microstrain), 2–5 per revolution, 2000 rpm, analysis.
[f]150 V rms effective = −141 to 282 V peak = 100 V rms with 2:1 bias.

The primary rotor design was for the active blade-tip configuration. The original design concept for the reconfiguration to the active twist rotor was to remove the blade tip from the actuator beam and lock the end of the actuator beam in a modified tip rib mounted in the outboard end of the main blade. This would result in a 90% diameter rotor, compared to the baseline design. This reconfiguration concept was successfully hover tested on the reduced tip speed rotor.[58] However, because of time constraints, it was not

possible to remove the active tip rotor from the test stand and reconfigure it in the described fashion. Instead, the blade tips were simply taped down to the main blade. Some actuation loss is expected across the taped joint; however, this was shown to be negligible below 3 per revolution.[55] A parametric design study indicated that at 2000 rpm, blade twist amplitudes of over ±1 deg can be readily achieved between 2–5 per revolution excitation at 330 microstrain (150 V rms).

The three main design objectives that were not completely met are 1) the target Mach number, 2) mass penalty, and 3) Lock number. All three of these are related to the growth in blade weight, associated with the actuator beam. The complete actuation system has a mass of 148 g, comprising 47.5% of the total blade mass. In conjunction with the higher blade mass, the rotor hub centrifugal load limit restricts the rotor speed to 2000 rpm. This translates to a tip Mach number of 0.47, which is slightly below the target range of Mach 0.55–0.6. The high rotor blade mass also contributes to the relatively low Lock number of 2.55, which results in reduced aerodynamic damping. In contrast, the bearingless Bell-412 and Boeing ITR model rotors have respective Lock numbers of 6.82 and 5.67.

Note, however, that compared to the first generation SABT-F97 rotor blade, the second-generation Mach-scale active tip rotor blade is 71 g (20%) lighter,[55] and there is room for further improvement with more detailed coupled actuator and rotor blade design and optimization studies. Note that the overall rotor design, in terms of blade planform, section profile, twist, and internal structure was motivated primarily by ease of fabrication. The aim of this research program was to demonstrate the active blade tip and active blade twist concept on a Mach-scale rotor. In particular, the objective was to evaluate the open-loop control authority of the active rotor, in terms of the rotating and fixed-frame hub loads. To this end, the rectangular blade and blade-tip planform, the single and symmetric profile, zero twist, and uniform structure (over the blade length) appear adequate and convenient. In future research, including full-scale design studies and investigation of forward flight performance, more advanced blade geometry and structural stiffness distribution need to be considered in the design optimization.

Design Layout

The design layout for the Mach-scale rotor model (Fig. 5) is based on the original SABT-F97 Froude-scale configuration,[58] with several key refinements. The primary instrumentation on the present rotor blades was a Hall sensor mounted on the shaft of the active blade tip (Fig. 5). The sensor was used in the active tip rotor configuration to measure the relative pitch rotation between the blade tip and the outboard end of the main blade. In the active twist configuration, this sensor was used to monitor the integrity of the taped junction between the outboard end of the main blade and the taped-down blade tips. Figures 6 and 7 show details of the fabricated rotor blades and components. In future tests, it is recommended to include blade torsional strain sensors and/or differential accelerometers to extract the piezo-induced blade twist (and to monitor torsional loads for fight safety).

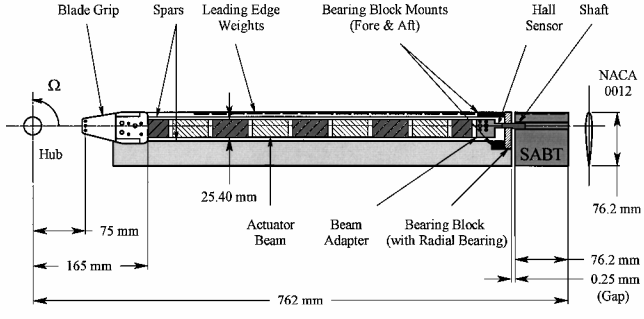

Fig. 5 Schematic of Mach-scale rotor blade with integrated actuator beam and active blade tip.

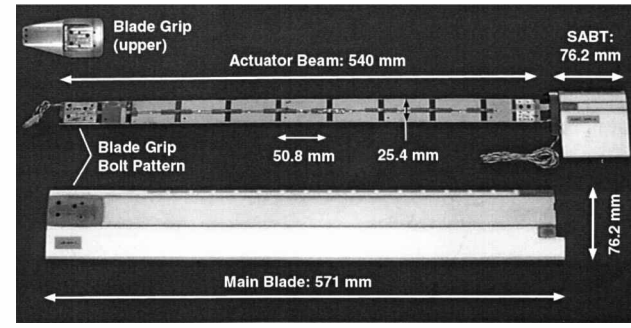

Fig. 6 Fabricated components for the Mach-scale active tip rotor, SABT-M99.

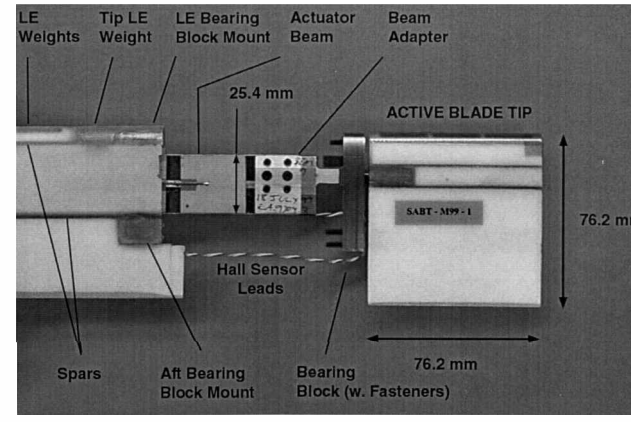

Fig. 7 Closeup of the actuator beam and blade tip, during assembly.

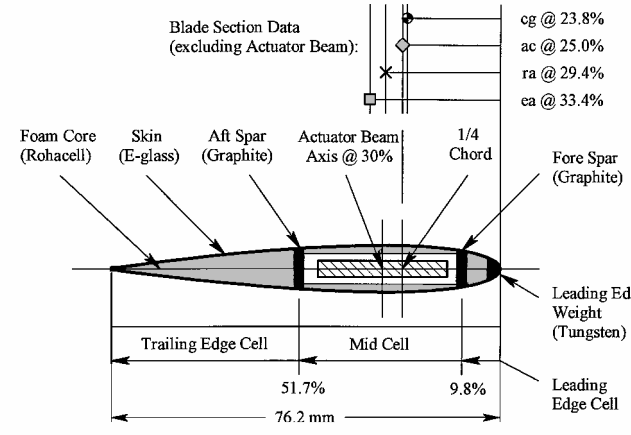

Fig. 8 Main blade cross section: aerodynamic center (ac), center of gravity (cg), elastic axis (ea), hub rotation axis X (ra), and shaft axis (sa).

Main Blade Cross Sections

A cross section through the main blade is shown in Fig. 8. The most important feature in terms of ease of fabrication and assembly is the three-cell cross section geometry with the actuator beam located spanwise in the hollow midcell. The outer skin is a plain weave [0,90] E-glass fabric, with three plies over the leading and midcells and one ply over the trailing edge cell. The dimensions shown in Fig. 8 represent the final configuration obtained after numerous design iterations. The location of the actuator beam is dictated primarily by the internal height required to accommodate the actuator beam and to provide sufficient clearance for the relative bending and twisting deformation.

Analytic Model

Figure 9 shows the finite element idealization of the active rotor blade. A general actuator beam finite element formulation was

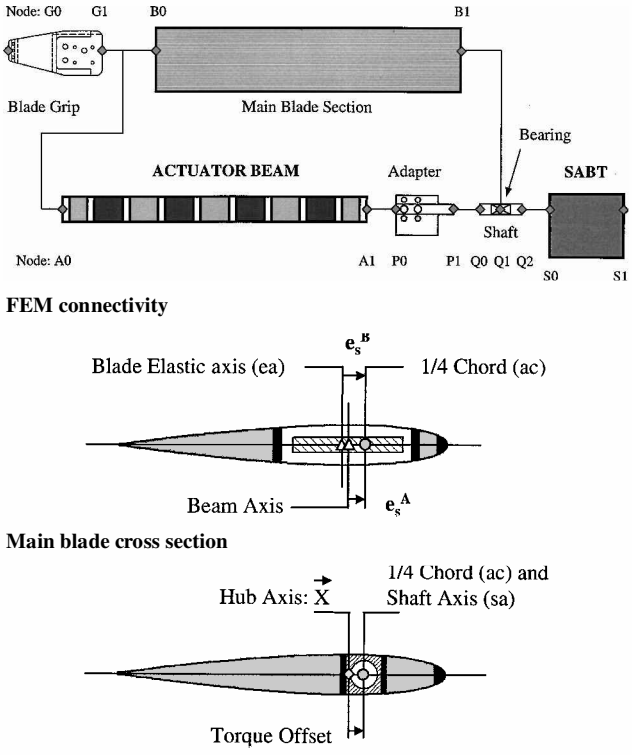

Fig. 9 FEM schematic.

developed, based on prior analytic work by Chandra and Chopra.[59] The analysis is an extension of Vlasov theory to include composite materials and induced-strain actuation. The actuator beam finite element model was integrated into a general aeroelastic rotor blade model, using Hamilton's variational principle. The coupling of the actuator beam, the main rotor blade, and the blade tip is via the boundary conditions between the three distinct structural components. The main rotor blade and blade tip are modeled using linear elasticity and linear aerodynamics. Two-dimensional unsteady aerodynamics are captured via the inclusion of noncirculatory impulsive aerodynamics and the correction of the circulatory lift via Theodorson's frequency-domain deficiency function. A uniform inflow model is used for the hover analysis. In addition, it is assumed that the inflow is independent of the blade-tip actuation.

The primary purpose of the coupled actuator beam and rotor blade analysis was to serve as a parametric design tool for the actuator beam and for evaluating the active blade-tip/blade-twist performance in hover. For more advanced design studies to investigate forward flight performance, full-scale feasibility and for design optimization, it is necessary to integrate the actuator beam structural model into a comprehensive aeroelastic rotor code.

The development of the specialized 12 degree-of-freedom actuator beam finite element (including induced-strain actuation capability), validation with bending–torsion test data in the literature and correlation with nonrotating experimental data of fabricated actuator beams are presented in detail in Refs. 55 and 57. The coupled actuator and rotor blade model was validated with hover test data of a reduced tip speed SABT rotor[60] and the Mach-scale SABT rotor.[54,55]

Nonrotating Tests

Figure 10 shows the nonrotating frequency sweep of the four active twist blades (clamped at the root). The blades were tested at excitation levels of 100 V rms with a bias settings up to 2:1, that is, ratio of poling to depoling direction electric field amplitude is 2:1, giving an effective voltage of 150 V rms. The results include five data sets. For the fifth data set, blade M99-02 was reconfigured with the blade tip removed and the beam locked in a modified tip rib (as originally envisaged), and designated SABTatwNT-M99-02 [no tip (NT)]. That data set serves primarily to demonstrate that there was no significant actuation loss (below resonance) associated with taping the blade tips down for the active twist hover test.

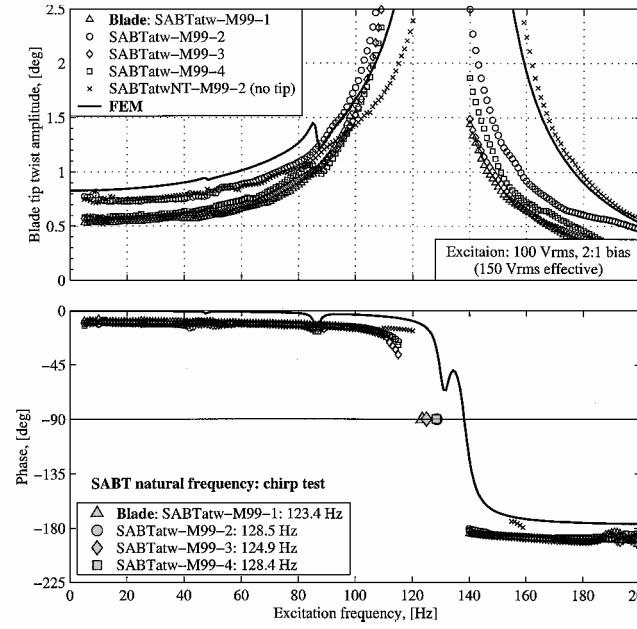

Fig. 10 Nonrotating blade twist frequency sweep, 150 V rms; blade-tip-twist amplitude is half-peak-to-peak, main blade clamped at root.

Only the dominant torsion mode was experimentally identified, by exciting the actuator beam with a 50 V rms chirp signal and using two differential laser-displacement sensors to measure tip twist response. The measured natural torsion frequencies are plotted on the −90 deg phase crossover line, for each blade, in Fig. 10. The experimental damping values for that mode range from 1.4 to 1.7%. The analysis overpredicts the dominant torsion frequency by 7.7–12.4%. The main reason is that the finite element model overpredicts the actuator beam torsional stiffness by 16%. (See Ref. 55 for further details.) The analytic phase drops in the torsion response at 86 and 130 Hz are related to coupling with dominant actuator bending modes.

Figure 10 shows that blade SABTatw-M99-2 has a superior blade twist capability compared to the other three blades. The low-frequency blade-tip twist amplitude is 0.78 deg (half-peak-to-peak), compared to 0.5–0.6 deg for the other three blades (37.5–25% lower). The reason that blade SABTatw-M99-2 outperforms the other blades is related to the blade not being extensively tested in the preceding active blade-tip configuration hover tests[55] (because of a blade-tip bearing problem). As a result of the prior testing at 150 V rms, there may have been some PZT cracking, resulting in reduced actuation capability. This is supported by actuator current measurements. The measured natural torsion frequencies of blades SABTatw-M99-1,3,4 do not evidence any stiffness loss associated with PZT cracking (when accounting for variations in average piezo thickness from beam to beam), probably because the change in stiffness is small compared to the combined beam and blade stiffness.

The finite element model (FEM) predicts a low-frequency blade-tip twist amplitude of 0.8 deg and overpredicts the measured SABTatw-M99-2 performance by approximately 10% up to 80 Hz. The reason for this is that the model overpredicts the actuator beam stiffness.[55] The tip twist amplitude increases to approximately 1.5 deg at 100 Hz. Because the fabricated beams have a lower natural frequency, the measured postresonance amplitude drops earlier than that predicted by the model. The measured blade-tip twist does, however, remain above 0.5 deg up to 166.7 Hz (5 per revolution at 2000 rpm).

The low-frequency data for blade SABTatw-NT-M99-2 (actuator beam clamped in a tip rib) is nearly identical to that of SABTatw-M99-2 (with the blade tip attached and taped down). This demonstrates that there is no significant actuation loss across the taped

junction preventing relative rotation between the blade tip and the outboard end of the main blade, at least for that particular blade and frequencies below 100 Hz. Without the blade-tip inertia, the active twist blade has a higher fundamental torsion frequency, measured at 146 Hz. The results indicate that good blade twist authority can be achieved, with correct locking of the actuator beam at the outboard end of the main blade, thereby indicating potential for further development.

Fan Diagram

Figure 11 shows the fan diagram for the Mach-scale active twist rotor, SABTatw-M99. The nonrotating data in the fan plot are based on impact hammer tests and chirp excitation of the active blade. The first three nonrotating blade flap modes are well captured. The dominant combined blade/actuator beam torsion mode (BAT1) is overpredicted by 7.7–12.4%. (See Ref. 55 for further details.) Rotating frame measurements were taken only at 2000 rpm. The first and second blade flap–bending frequencies were from the active twist frequency sweeps and correlate well with the FEM predictions. The data points shown, include the tests of all four blades at three collective settings of 4, 6, and 8 deg, respectively. The first flap frequency is overpredicted by up to 5.2%, and the second flap frequency by up to 0.5%.

For completeness, the rotating rotor blade mode shapes are included in Fig. 12 and the corresponding actuator beam mode shapes in Fig. 13. The plots vividly display the highly coupled nature of the actuator–beam and rotor–blade system (related to the bending–torsion structural coupling of the actuator beam and the inertial bending–torsion coupling of the main blade). Note that at the blade and actuator beam junction (at 21 and 90%R) the blade mode shapes and actuator mode shapes line up. The actuator beam mode shapes include a chordwise warping degree of freedom. This is essential to capture accurately the induced-strain actuation of the segmented bending–torsion actuator. (See Ref. 57 for further details.) Rotating mode shapes for modes 3–5 (at 3.54, 4.09, and 4.60 per revolution) show a strong torsion response. With comparison to uncoupled rotating mode shapes (not shown), it can be shown that the mode at 3.54 per revolution is a coupled bending–torsion mode related to actuator first flatwise bending (AF1). The mode at 4.09 per revolution is the dominant torsion mode of the combined actuator and main blade (BAT1). The mode at 4.60 per revolution is a flap–torsion coupled mode, originating from the third blade flap bending (BF3).

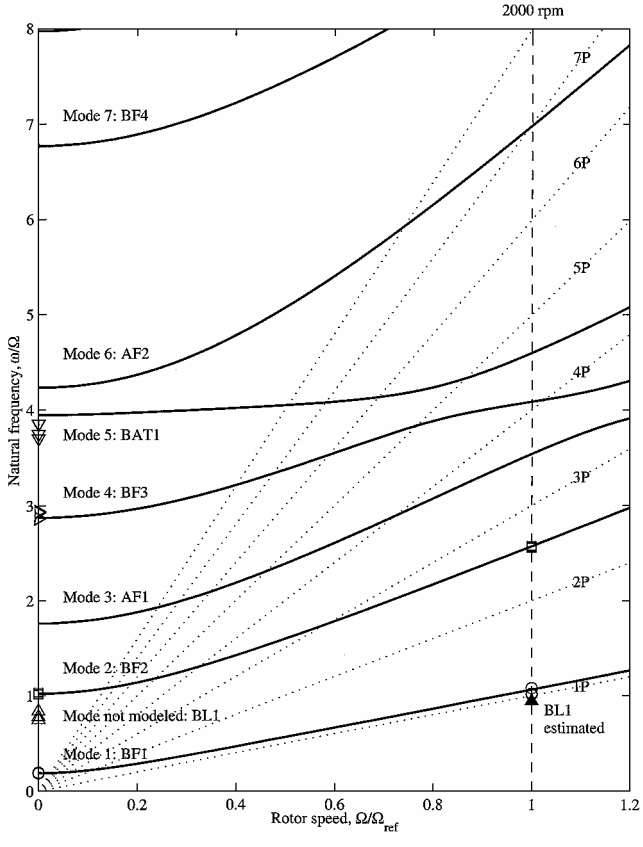

Fig. 11 Fan diagram: Mach-scale active twist rotor, SABTatw-M99, nominal speed 2000 rpm; descriptor is mode origin, B is blade, A is actuator, F is flap, L is lag, and T is torsion.

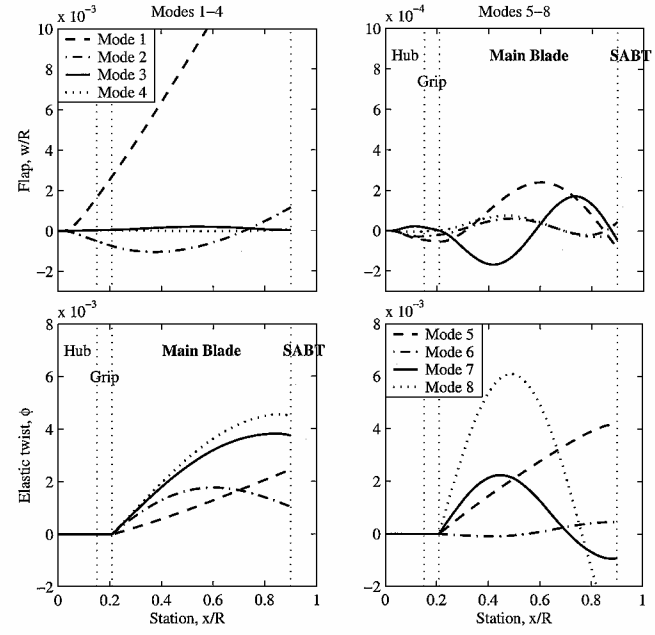

Fig. 12 Rotating blade mode shapes at 2000 rpm.

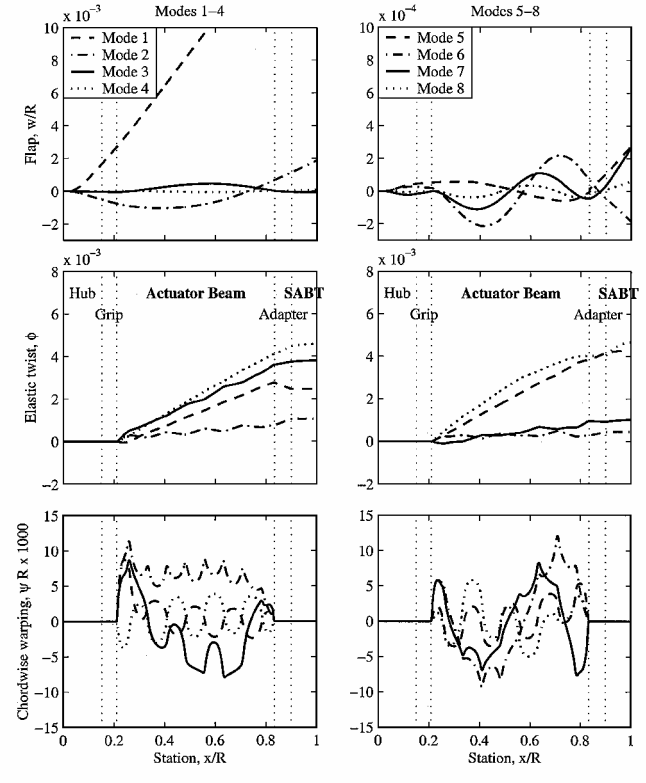

Fig. 13 Rotating actuator beam mode shapes at 2000 rpm.

Hover Tests

The open-loop hover tests were conducted at 2000 rpm (nominal tip Mach 0.47) with collective settings of 4, 6, and 8 deg. Note that in the present tests the rotor blades did not include any sensors to measure blade-tip twist (such as differential accelerometers or blade

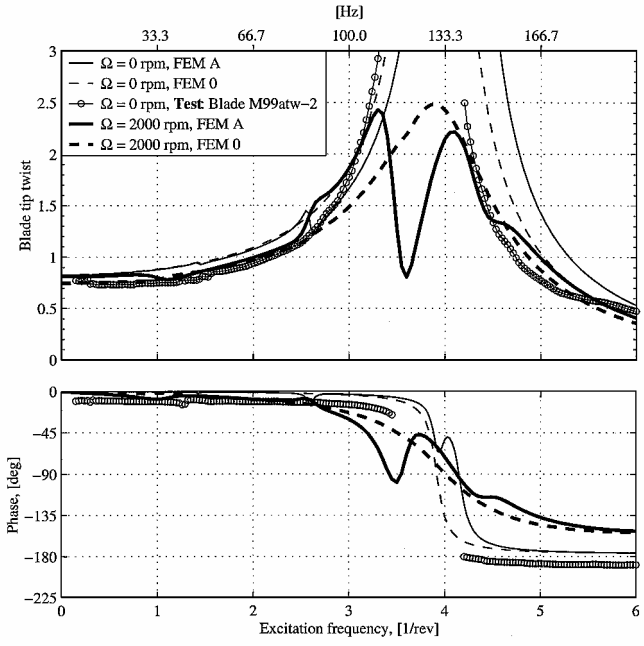

Fig. 14 Blade twist frequency sweep: 150 V rms; FEM A is baseline analysis, FEM 0 is analysis excluding offsets between the blade and beam axes; amplitude is half-peak-to-peak.

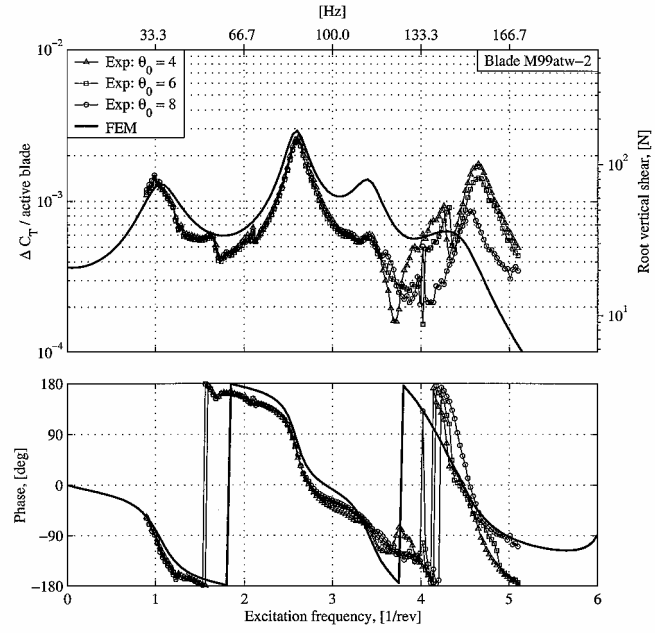

Fig. 15 Thrust frequency response: single blade actuation, hover, 2000 rpm, 150 V rms, blade SABTatw-M99-2.

root torsional strain gauges) because the primary focus was on the active blade-tip rotor configuration.

Figure 14 compares the predicted nonrotating and rotating blade-tip twist. Figure 14 includes the nonrotating experimental data for blade SABTatw-M99-2. The analysis is presented for two FEMs: FEM A and FEM 0. The first model, FEM A, includes all of the offsets between the blade and beam axes and, hence, includes the associated inertial and kinematic beam/blade flap/torsion couplings. In contrast, the second model, FEM 0, assumes that all of the axes are coincident on the quarter chord (eliminating the axes offset inertial and kinematic couplings and retaining only the structural bending–torsion coupling of the actuator beam). This model is included to demonstrate the performance in the absence of the couplings associated with the axes offsets. See Fig. 8, for the relative location of the respective blade, beam, and shaft axes.

The measured nonrotating, low-frequency blade-tip twist is 0.78 deg. The FEM results predict a quasi-static, nonrotating blade-tip twist of 0.83 deg, which overpredicts the measurement by 6.4%. Between 10 and 100 Hz, the nonrotating FEM results are within 0.13 deg of the measured blade-tip twist. Above 100 Hz, the analytic and experimental results differ more because the FEM overpredicts the beam torsional stiffness, and, hence, the predicted resonant amplification is delayed to a slightly higher frequency.

Compare the FEM A results for 0 rpm and full speed (2000 rpm): The predicted rotating blade-tip twist up to 0.8 per revolution (26.7 Hz) is within in 3% of the estimated nonrotating blade-tip twist. This indicates that no significant performance degradation is expected in moving from the nonrotating to rotating environment. The 3% actuation reduction is associated with centrifugal torsional stiffening of the rotor blade (and to a lesser extent the actuator beam). Beyond 0.8 per revolution, the difference in nonrotating and rotating dynamics comes into effect and the blade-tip-twist responses begin to differ more. Even then, from 0.8 to 3 per revolution, it is predicted that the 0- and 2000-rpm blade twist are within 0.2 deg. The predicted hover tip twist amplitudes at the rotor harmonics are 0.8 deg at 1 per revolution, 1.0 deg at 2 per revolution, 1.9 deg at 3 per revolution, 2.2 deg at 4 per revolution, and 1.0 deg at 5 per revolution.

The aerodynamic pitch damping at 2000 rpm brings the estimated resonant amplitudes down to 2.5 deg. In the presence of the various axes offsets, FEM A predicts a damped peak of 2.43 deg at 3.3 per revolution and another peak of 2.22 deg at 4.1 per revolution. The former peak is related to the coupling with the first flatwise bending mode of the actuator beam (AF1) and the latter peak is the first combined blade/beam torsion mode (BAT1). In the absence of the axes-offset inertial and kinematic couplings, FEM 0 predicted rotating blade-tip-twist response shows only one dominant resonance near 4 per revolution (−90 deg phase cross over at 4.05 per revolution, damped natural frequency at 3.9 per revolution), with a peak amplitude of 2.5 deg.

In future tests, it is important to include blade torsional strain sensors and/or differential accelerometers to extract the piezo-induced blade tip twist (and to monitor torsional loads for fight safety).

The response of the rotor normal force frequency response to single blade actuation is shown in Fig. 15 (for blade SABTatw-M99-2, 2000 rpm hover). At 8 deg collective, and for a single blade actuation of 150 V rms at 1, 2, and 3 per revolution, respectively, the measured oscillatory thrust coefficients are 1.4×10^{-3}, 0.55×10^{-3}, and 0.7×10^{-3}. That corresponds to 25, 10, and 13% of the measured rotor thrust (at 8 deg collective). Up to 3.5 per revolution, there is no discernible difference between the thrust response at 4, 6, and 8 deg collective. The thrust response of the active twist rotor is dominated by inertial loads (rather than aerodynamic loads) because of low damping resulting from the low Lock number. Consequently, a high oscillatory thrust authority is demonstrated.

The FEM accurately captures the experimental measurements up to approximately 2.9 per revolution (just past the second rotor flap frequency, BF2). Beyond 3 per revolution, however, the analysis and the experimental results differ. It can be shown analytically[55] that near the actuator–beam first flatwise-bending mode, located at 3.54 per revolution (FEM A), the beam impacts the main blade. The beam/blade interference problem can be readily eliminated in future research by placing a (torsionally free) bending support between the actuator beam and the main blade near the midspan, effectively stiffening the beam bending modes. For example, the beam can be split in two with a central junction shaft supported in a radial bearing.

Furthermore, actuation losses across the taped junction were also noted above 3 per revolution. In the active blade-tip configuration, a Hall sensor is used to measure the pitch angle of the blade tip relative to the outboard end of the main blade. In the active twist configuration, with the blade tip taped down, the Hall sensor measurement is an indication of the actuation loss across the taped junction. The experimental results (not shown) indicate that between 3 and 4.4 per revolution the taped junction is not completely effective and that there is a relative twisting between the blade tip and the main blade, on the order of 0.1–0.3 deg. It is, therefore, expected

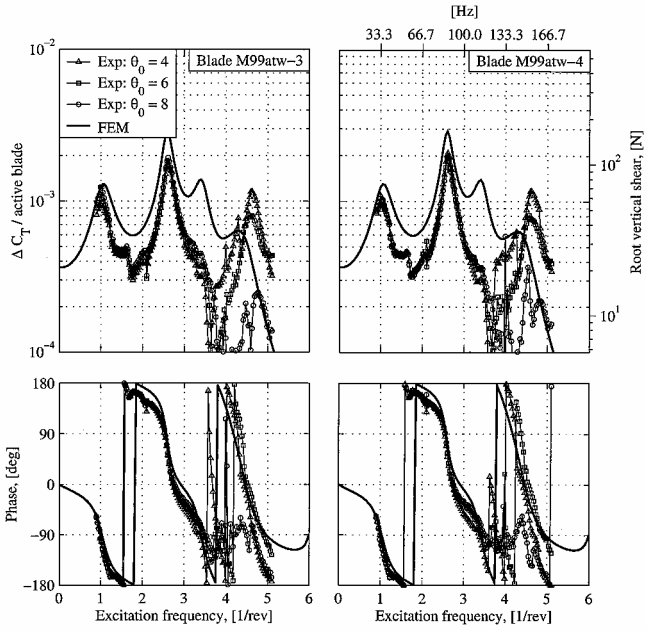

Fig. 16 Thrust frequency response: single blade actuation, hover, 2000 rpm, 150 V rms, blades SABTatw-M99-3 and M99-4, respectively.

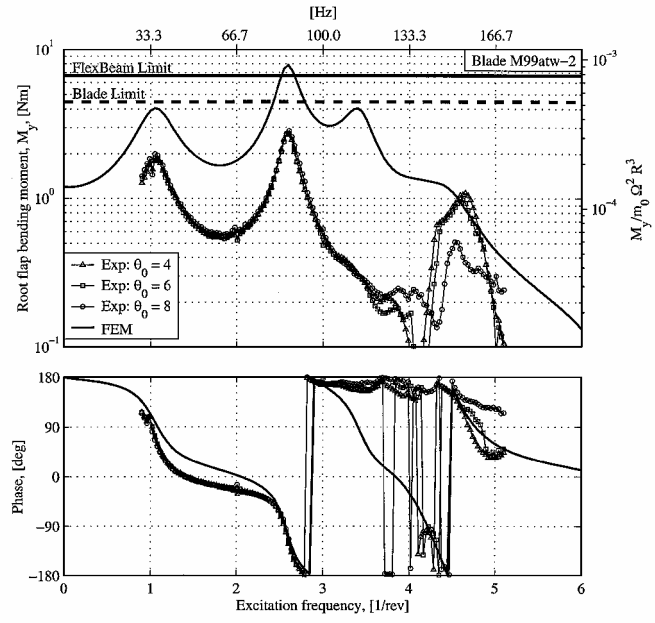

Fig. 17 Root flap bending moment frequency response: hover, 2000 rpm, 150 V rms, blade SABTatw-M99-2.

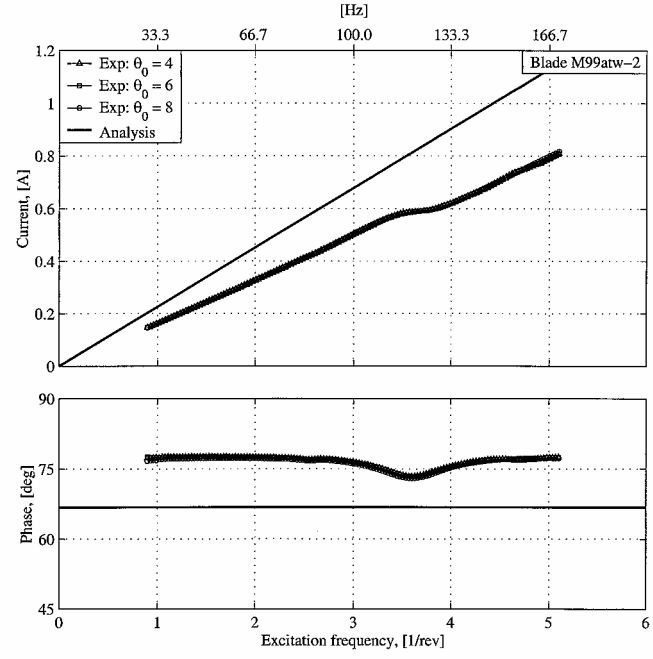

Fig. 18 Active twist frequency sweep (hover, 2000 rpm): actuator current, 150 V rms; blade SABTatw-M99-2, amplitude half-peak-to-peak.

that the measured and predicted normal force results will differ between 3 and 4 per revolution, because of beam/blade interference and actuation losses across the taped junction.

Figure 16 shows the induced-thrust generated by blades SABTatw-M99-3 and SABTatw-M99-4, respectively. These blades demonstrate a lower thrust authority compared to blade SABT-M99-2 because of the 20–30% lower twist actuation capability noted in the nonrotating bench tests (Fig. 10). The most likely reason for the performance reduction is that blades M99-1,-3,-4 were extensively hover tested in active tip configuration before the active twist tests. Blade M99-2 suffered severe bearing lock, even at low collective settings, and was not significantly tested in active tip mode. It is surmised that the more exhaustively tested blades M99-1, M99-3, and M99-4, incurred piezo-cracking damage during the 150-V rms actuation tests.

Blade SABT-M99-2 was probably also protected further, by its actuator beam (AB-M99-10) having the thickest piezoelements (5% thicker than the 0.254 mm average) and, hence, was exposed to 5% lower electric fields (for a given voltage setting). The presence of piezo damage in the actuator beams in blades M99-1-,3-,-4 is supported by the fact that the current drawn by the actuator beams in hover is lower than that measured during the initial nonrotating characterization tests of the active blade-tip rotor blades.[55] (Those tests were conducted before the active twist test campaign.)

The blade root flap bending moment for the SABTatw-M99-2 active twist frequency sweep is given in Fig. 17. Similar to the active tip tests[54,55] the FEM captures the trend over the two blade flap frequencies, but significantly overpredicts the measured root-flap bending moment. After the hover test, the flap bending gauges were retested statically and found to be within acceptable limits of the pretest calibration. The reason for this discrepancy requires further investigation. As a first step, it is recommended to compare the flap bending moment predictions from the present analysis with those from a suitably modified comprehensive aeroelastic rotor code.

The actuator current requirements for the active twist tests are shown in Figs. 18 and 19. Peak measured actuator current, at 5 per revolution and 150 V rms, is between 0.8 and 1.0 A. This corresponds to an average power consumption of up to 71 W per actuator beam (assuming that all power discharged by the actuator is dissipated) and represents 1.6% of the (aerodynamic) main rotor power at 8 deg collective. When suitable power electronics are used, the power consumption can be further reduced because of the predominant reactive power characteristic.

The analysis of the actuator current is based on modeling piezoceramic elements as lossy capacitors. (See Refs. 55 and 61 for details.) The analysis overpredicts the measurements because the field-dependent variation of the transverse permittivity and the loss factors were extrapolated from Ref. 61. Hence, the analytic line should be considered as a guideline only. Further piezoceramic material testing is required to extract the relevant parameters over the full operating range to enhance the validity of the analysis.

When the actuator current measured in successive tests sets is compared, it can be seen that the current has decreased as the tests progressed. (Test sequence was 8 deg collective followed by 6 and then 4 deg.) This is most pronounced for blade M99-3, whose actuator beam has the thinnest piezoceramics, on average 5% less than the 0.254 mm nominal thickness. The thinner PZTs experience higher stress levels associated with the centrifugal tension.

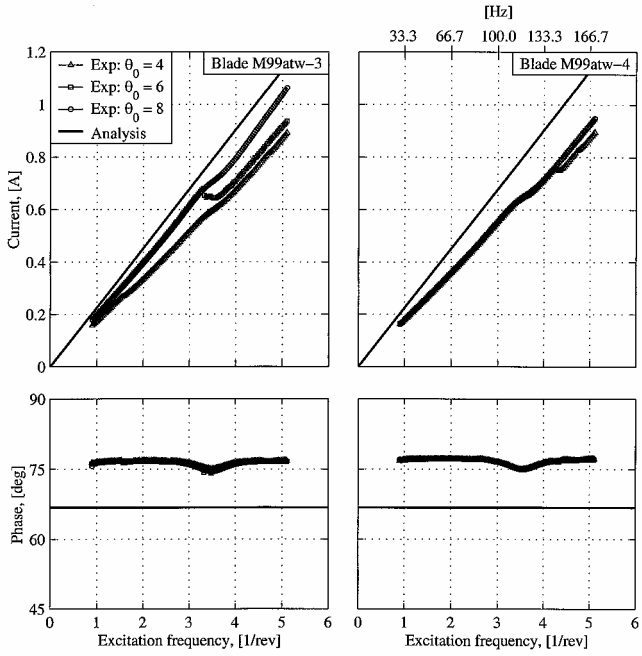

Fig. 19 Active twist frequency sweep (hover, 2000 rpm): actuator current, 150 V rms, blades SABTatw-M99-3 and M99-4, amplitude half-peak-to-peak.

Furthermore, for a given excitation voltage, the thinner PZTs see a 5% higher electric field and a disproportionately higher freestrain. Consequently the actuator beam with the thinner piezoceramic elements is more susceptible to piezo cracking. After the frequency sweeps, the capacitance of the actuator beams was rechecked, and surface resistance measurements of the piezoelectrodes were taken (corner-to-corner). Blade SABTatw-M99-3 showed a 10% drop in capacitance, although the capacitance of the other three actuator beams was similar to that measured before hover testing. The surface resistance measurements showed a three- to fourfold increase from a nominal value of 2 Ω ohm to 6–8 Ω. The latter measurement indicates the presence of micro-cracks in the full-surface Nickel electrode on the PZT element. It is surmised that, on actuation and/or under rotation, the PZT cracks, or at least the cracks in the surface electrodes, open slightly, thereby effectively cutting a portion of the PZT off from the excitation field. This explains the lower nonrotating twist actuation of blades M99-1,-3,-4 shown in Fig. 10.

In the design stage, the preliminary structural integrity analysis indicated that piezo cracking was likely in the piezoceramics near the beam root at drive voltages of 100 V rms with 2:1 bias (150 V rms effective). There are two potential remedies to mitigate piezo cracking in subsequent research. The first is to separate the active tip and active twist rotor designs, optimizing each separately. In the latter, the main blade is lengthened and the blade tip removed. The actuator beam is locked in a rib at the outboard end of the main blade. When the blade tip is removed (which in the present design is supported axially by the actuator beam), the tension load in the actuator beam is significantly reduced resulting in commensurately lower tensile stress levels in the piezoelements. For example, for the present design, simply by removing the blade tip, the tension at the root of the actuator beam at 2000 rpm is reduced by 35%. It is also proposed to consider PZT precompression techniques during bonding, to further lower mean tensile stress levels in the piezoelements.

The preceding hover-test results demonstrate that the piezo-induced bending–torsion beam can generate appreciable active blade twist and alter the blade root flap-bending moment and root vertical shear and, hence, the hub loads. The difficulties with piezo cracking and impacting of the actuator beam within the blade mid-cell can be negated by suitable design changes. With a dedicated design optimization for the active twist configuration (rather than a piggy-back design to the active blade-tip rotor), it is expected that the active twist performance and system integrity can be significantly improved.

Conclusions

The active twist rotor presented in this research is a derivative of the previously developed and tested smart active blade-tip rotor. When the blade tips are locked to the main blade, the actuator beam twists the entire blade. Nonrotating tests demonstrated a low frequency blade-tip-twist amplitude of 0.78 deg under an excitation of 150 V rms, for one of the four rotor blades. The other two blades that were tested showed approximately 25% lower performance. It is surmised that the main reason for the performance difference is that the latter two blades were extensively tested in the active blade-tip configuration before the active twist tests. High electro-mechanical loads most likely resulted in cracking of some of the PZT elements and, hence, performance degradation. Below 100 Hz, the analytic tip twist is within 0.13 deg of the measured results of blade M99-2. The analysis indicates that no significant performance reduction is expected at 2000 rpm compared to zero rpm.

In 2000-rpm hover, good correlation of the analysis and measured rotor thrust is obtained up to 3 per revolution actuation. The measured oscillatory blade lift (for single blade actuation) was 79, 32, and 43 N at 1, 2, and 3 per revolution, respectively. Compared to a measured steady 8 deg rotor thrust of 315 N, thrust authority in excess of 10% is achievable (per active blade). Beyond 3 per revolution, actuation losses associated with elastic losses across the taped main blade and blade-tip junction and beam/blade interference were noted.

In assessing the active twist performance note the following.

1) The rotor blade and actuator were neither designed nor optimized for the active twist role. In particular, the actuator beam and main blade are not stiffness matched. For the present design, the ratio of the beam/blade equivalent uniform torsional stiffnesses is 63.6%.

2) The blade tip was simply taped down to the main blade, to facilitate rapid evaluation of the active twist performance. Elastic losses in the taped joint resulted in performance degradation above 3 per revolution. This can be eliminated by removing the blade tip and securely locking the beam in a dedicated tip rib.

3) Furthermore, with the blade tip removed, the tension in the actuator beam root is reduced by 35%, and it is possible to safely actuate the beam at 150 V rms, even without PZT precompression (without risk of piezo cracking).

When the preceding points are taken into consideration, there is significant room to improve the active twist design and achieve enhanced performance. The hover test demonstrates the potential of the active twist rotor system using an internal actuation beam and warrants further research for a dedicated next-generation Mach-scale design and full-scale feasibility study.

Acknowledgment

This work is supported by the U.S. Army Research Office under the Multi University Research Initiative Grant DAAH-04-096-10334 with Tom Doligalski and Gary Anderson as Technical Monitors.

References

[1] Chopra, I., "Status of Application of Smart Structures Technology to Rotorcraft Systems," *Journal of the American Helicopter Society*, Vol. 45, No. 4, 2000, pp. 228–252.

[2] Straub, F. K., "A Feasibility Study of Using Smart Materials for Rotor Control," *Smart Materials and Structures*, Vol. 5, No. 1, 1996, pp. 1–10.

[3] Straub, F. K., and Merkley, D. J., "Design of a Smart Material Actuator for Rotor Control," *Smart Materials and Structures*, Vol. 6, No. 3, 1997, pp. 223–234.

[4] Jacot, D., "Smart Structures for Rotorcraft Control (SSRC)," *4th Symposium on Smart Structures and Materials, Conference on Industrial and Commercial Applications of Smart Structures Technologies*, Vol. 3044, edited by J. M. Sater, Society of Photo-Optical Instrumentation Engineers, Bellingham, WA, 1997, pp. 114–122.

[5] Loewy, R., "Recent Developments in Smart Structures with Aeronautical Applications," *Smart Materials and Structures*, Vol. 6, No. 5, 1997, pp. R11–R42.

[6]Giurgiutiu, V., "Recent Advances in Smart-Material Rotor Control Actuation," AIAA Paper 2000-1709, April 2000.

[7]Koratkar, N., Spencer, M. G., and Chopra, I., "Wind Tunnel Testing of a Mach-Scaled Active Rotor with Trailing-Edge Flaps," *American Helicopter Society 57th Annual Forum*, Washington, DC, May 2001.

[8]Koratkar, N. A., and Chopra, I., "Wind Tunnel Testing of a Mach-Scaled Rotor Model with Trailing Edge Flaps," *Smart Materials and Structures*, Vol. 10, No. 1, 2001.

[9]Koratkar, N. A., "Smart Helicopter Rotor with Piezoelectric Bender Actuated Trailing-Edge Flaps," Ph.D. Dissertation, Aerospace Engineering Dept., Univ. of Maryland, College Park, MD, Nov. 2000.

[10]Fulton, M., and Ormiston, R. A., "Hover Testing of a Small-Scale Rotor with On-Blade Elevons," *Journal of the American Helicopter Society*, Vol. 46, No. 2, 2001, pp. 96–106.

[11]Fulton, M., and Ormiston, R. A., "Small-Scale Rotor Experiments with On-Blade Elevons to Reduce Blade Vibratory Loads in Forward Flight," *American Helicopter Society 54th Annual Forum*, Washington, DC, May 1998.

[12]Prechtl, E. F., and Hall, S. R., "Closed-Loop Vibration Control Experiments on a Rotor with Blade Mounted Actuation," AIAA Paper 2000-1714, April 2000.

[13]Prechtl, E. F., "Design and Implementation of a Piezoelectric Servo-Flap Actuation System for Helicopter Rotor Individual Blade Control," Ph.D. Dissertation, Dept. of Aeronautics and Astronautics, Massachusetts Inst. of Technology, Cambridge, MA, Feb. 2000.

[14]Straub, F., "Development of an Active Flap Rotor," *9th ARO International Conference on Aeroelasticity of Rotorcraft Systems*, Ann Arbor, MI, Oct. 2001.

[15]Straub, F. K., Ngo, H., Anand, V., and Domzalski, D., "Development of a Piezoelectric Actuator for Trailing Edge Flap Control of Full Scale Rotor Blades," *Smart Materials and Structures*, Vol. 10, No. 1, 2001, pp. 25–**XX**.

[16]Hall, S. R., Tzianetopoulou, T., Straub, F. K., and Ngo, H. T., "Design and Testing of a Double X-Frame Piezoelectric Actuator," *Proceedings of SPIE's 7th Symposium on Smart Structures and Materials, Conference on Smart Structures and Integrated Systems*, Vol. 3985, edited by N. M. Wereley, Society of Photo-Optical Instrumentation Engineers, Bellingham, WA, 2000, pp. 26–37.

[17]Lee, T., and Chopra, I., "Development and Validation of a Refined Piezostack-Actuated Trailing-Edge Flap Actuator for a Helicopter Rotor," *SPIE's 6th Symposium on Smart Structures and Materials, Conference on Smart Structures and Integrated Systems*, Vol. 3668, edited by N. M. Wereley, Society of Photo-Optical Instrumentation Engineers, Bellingham, WA, 1999, pp. 22–36.

[18]Lee, T., "Design of a High Displacement Smart Trailing Edge Flap Actuator Incorporating Dual-Stage Mechanical Stroke Amplifiers for Rotors," Ph.D. Dissertation, Aerospace Engineering Dept., Univ. of Maryland, College Park, MD, Dec. 1999.

[19]Jänker, P., "Smart Structures at EADS Corporate Research Center," *12th International Conference on Adaptive Structures and Technologies (ICAST)*, College Park, MD, Oct. 2001.

[20]Jänker, P., Klöppel, V., Hermle, F., Lorkowski, T., Storm, S., Christmann, M., and Wettemann, M., "Development and Evaluation of a Hybrid Piezoelectric Actuator for Advanced Flap Control Technology," *25th European Rotorcraft Forum*, Paper G-21, Sept. 1999.

[21]Hasegawa, Y., Hatayama, N., Kobiki, N., and Nakasto, E., "Experimental and Analytic Results of Whirl Tower Test of ATIC Full Scale Rotor System," *American Helicopter Society 57th Annual Forum*, Washington, DC, May 2001.

[22]Fink, D. A., Hawkey, T. J., and Gaudreau, M. P., "An Electromagnetic Actuator for Individual Blade Control," *American Helicopter Society 56th Annual Forum*, Virginia Beach, VA, May 2000.

[23]Domzalski, D., "Application of Smart Structures Technology to Stability Augmentation and Vibration Reduction in Rotorcraft," *9th ARO International Conference on Aeroelasticity of Rotorcraft Systems*, Ann Arbor, MI, Oct. 2001.

[24]Chen, P. C., and Chopra, I., "Wind Tunnel Test of a Smart Rotor Model with Individual Blade Twist Control," *Journal of Intelligent Material Systems and Structures*, Vol. 8, No. 5, 1997, pp. 414–425.

[25]Chen, P. C., and Chopra, I., "Hover Test of a Smart Rotor with Induced Strain Actuation of Blade Twist," *AIAA Journal*, Vol. 35, No. 1, 1997, pp. 6–16.

[26]Chen, P. C., "Development of a Smart Rotor with Induced-Strain Actuation of Blade Twist," Ph.D. Dissertation, Aerospace Engineering Dept., Univ. of Maryland, College Park, MD, 1996.

[27]Bernhard, A. P., and Chopra, I., "Hover Test of a Mach-Scale Active-Twist Rotor Using Piezo-Induced Bending–Torsion Actuator Beams," American Helicopter Society North-East Region National Technical Specialists' Meeting on Active Rotor Technology, Bridgeport, CT, Oct. 2000.

[28]Rodgers, J. P., and Hagood, N. W., "Preliminary Mach-Scale Hover Testing of an Integral Twist-Actuated Rotor Blade," *SPIE's 5th Symposium on Smart Structures and Materials, Conference on Smart Structures and Integrated Systems*, Vol. 3329, edited by M. E. Regelbrugg, Society of Photo-Optical Instrumentation Engineers, Bellingham, WA, 1998, pp. 291–308.

[29]Rodgers, J. P., "Development of an Integral Twist-Actuated Rotor Blade for Individual Blade Control," Ph.D. Dissertation, Dept. of Aeronautics and Astronautics, Massachusetts Inst. of Technology, Cambridge, MA, Oct. 1998.

[30]Wilbur, M. L., Mirick, P. H., Yeager, W. T., Langston, C. W., Cesnik, C. E., and Shin, S., "Vibratory Loads Reduction Testing of the NASA/ARMY/MIT Active Twist Rotor," *American Helicopter Society 57th Annual Forum*, Washington, DC, May 2001.

[31]Wilbur, M. L., Yeager, W. T., Wilkie, W. K., Cesnik, C. E., and Shin, S., "Hover Testing of the NASA/ARMY/MIT Active Twist Rotor Prototype Blade," *American Helicopter Society 56th Annual Forum*, Virginia Beach, VA, May 2000.

[32]Derham, R., Weems, D., Mathew, M. B., and Bussom, R., "The Design Evolution of an Active Materials Rotor," *American Helicopter Society 57th Annual Forum*, Washington, DC, May 2001.

[33]Büter, A., Ehlert, U., and Breitbach, E., "Adaptive Rotor Blade for Vibration Reduction," *9th ARO International Conference on Aeroelasticity of Rotorcraft Systems*, Ann Arbor, MI, Oct. 2001.

[34]Ormiston, R., "Aeroelastic Considerations for Rotorcraft Primary Flight Control with On-Blade Elevons," *American Helicopter Society 57th Annual Forum*, Washington, DC, May 2001.

[35]Shen, J., and Chopra, I., "Stability and Loads of Helicopter Rotor with Smart Flaps for Primary Control," *9th ARO International Conference on Aeroelasticity of Rotorcraft Systems*, Ann Arbor, MI, Oct. 2001.

[36]Barrett, R., "All-Moving Active Aerodynamic Surface Research," *Smart Materials and Structures*, Vol. 4, No. 2, 1995, pp. 65–74.

[37]Barrett, R., and Brozoski, F., "Adaptive Flight Control Surfaces, Wings, Rotors and Active Aerodynamics," *SPIE's 3rd Symposium on Smart Structures and Materials, Conference on Smart Structures and Integrated Systems*, Vol. 2717, edited by I. Chopra, Society of Photo-Optical Instrumentation Engineers, Bellingham, WA, 1996, pp. 178–198.

[38]Barrett, R., Schliesman, M., and Frye, P., "Design, Development and Testing of a Mini Solid State Adaptive Rotorcraft," *SPIE's 4th Symposium on Smart Structures and Materials, Conference on Smart Structures and Integrated Systems*, Vol. 3041, edited by M. E. Regelbrugge, Society of Photo-Optical Instrumentation Engineers, Bellingham, WA, 1997, pp. 231–242.

[39]Bent, A. A., and Hagood, N. W., "Anisotropic Actuation with Piezoelectric Fiber Composites," *Journal of Intelligent Material Systems and Structures*, Vol. 6, No. 3, 1995, pp. 338–349.

[40]Rodgers, J. P., and Hagood, N. W., "Manufacture of Adaptive Composite Plates Incorporating Piezoelectric Fiber Composite Plies," *36th AIAA/ASME/ASCE/AHS/ASC Structures, Structural Dynamics, and Materials Conference and AIAA/ASME Adaptive Structures Forum*, AIAA, Washington, DC, 1995, pp. 2824–2835.

[41]Rodgers, J. P., Bent, A. A., and Hagood, N. W., "Characterization of Interdigitated Electrode Piezoelectric Fiber Composites Under High Electrical and Mechanical Loading," *SPIE's 3rd Symposium on Smart Structures and Materials, Conference on Smart Structures and Integrated Systems*, Vol. 2717, edited by I. Chopra, Society of Photo-Optical Instrumentation Engineers, Bellingham, WA, 1996, pp. 642–659.

[42]Strock, H., Pascucci, M., Parish, M., and Bent, A., "Active PZT Fibers: A Commercial Production Process," *SPIE's 6th Symposium on Smart Structures and Materials, Conference on Smart Materials Technologies*, Vol. 3668, edited by N. M. Wereley, Society of Photo-Optical Instrumentation Engineers, Bellingham, WA, 1999, pp. 22–31.

[43]Derham, R. C., and Hagood, N. W., "Rotor Design Using Smart Materials to Actively Twist Blades," *American Helicopter Society 52nd Annual Forum*, Washington, DC, 1996, pp. 1242–1252.

[44]Rodgers, J. P., Hagood, N. W., and Weems, D., "Design and Manufacture of an Integral Twist-Actuated Rotor Blade," *38th AIAA/ASME/ASCE/AHS/ASC Structures, Structural Dynamics, and Materials Conference and AIAA/ASME/AHS Adaptive Structures Forum*, Kissimmee, FL, 1997.

[45]Wilkie, W. K., Wilbur, M. L., Mirick, P. H., Cesnik, C. E., and Shin, S., "Aeroelastic Analysis of the NASA/ARMY/MIT Active Twist Rotor," *American Helicopter Society 55th Annual Forum*, Montreal, Canada, May 1999.

[46]Cesnik, C. E., Shin, S., Wilkie, W. K., Wilbur, M. L., and Mirick, P. H., "Modeling, Design and Testing of the NASA/ARMY/MIT Active Twist Rotor Prototype Blade," *American Helicopter Society 55th Annual Forum*, Montreal, Canada, May 1999.

[47]Cesnik, C. E., and Shin, S., "On the Twist Performance of a Multiple-Cell Active Helicopter Blade," *Smart Materials and Structures*, Vol. 10, No. 1, 2001, pp. 53–61.

[48]Cesnik, C. E., Shin, S., and Wilbur, M., "Dynamic Response of Active Twist Rotor Blades," *Smart Materials and Structures*, Vol. 10, No. 1, 2001, pp. 62–76.

[49]Wickramasinghe, V., and Hagood, N., "Material Characterization of Active Fiber Composite Actuators for Active Twist Helicopter Rotor Blade Applications," AIAA Paper 2000-1709, April 2000.

[50]Wilkie, W. K., Bryant, R. G., High, J. W., Fox, R. L., Hellbaum, R. F., Jalink, A., Little, B. D., and Mirick, P. H., "Low-Cost Piezocomposite Actuator for Structural Control Application," *Society of Photo-Optical Instrumentation Engineers 7th Symposium on Smart Structures and Materials, Conference on Smart Structures and Integrated Systems*, Vol. 3991, edited by J. H. Jacobs, March 2000.

[51]Büter, A., Breitbach, E., and Hanselkar, H., "The Main Sources of Helicopter Vibration and Noise Emissions and Adaptive Concepts to Reduce Them," *Innovation in Rotorcraft Technology*, Royal Aeronautical Society, London, 1997, pp. 12.1–12.9.

[52]Büter, A., "Untersuchung Adaptiver Konzepte zur Reduktion von Hubschraubervibrationen, zur Minderung des Hubschrauberl ärms und zur Steigerung der aerodynamischen Effizienz," Ph.D. Dissertation, Technical Rept. FB-98-12, Deutsches Zentrum für Luft- und Raumfahrt e.V., May 1998.

[53]Bernhard, A. P., and Chopra, I., "Hover Testing of an Active Rotor Blade Tip and Structural Analysis of the Actuator Beam," *39th AIAA/ASME/ASCE/AHS/ASC Structures, Structural Dynamics, and Materials Conference and AIAA/ASME/AHS Adaptive Structures Forum*, AIAA, Reston, VA, 1998, pp. 3299–3325.

[54]Bernhard, A. P., and Chopra, I., "Hover Test of a Mach-Scale Rotor-Model with Active Blade Tips," *Journal of the American Helicopter Society* (accepted for publication).

[55]Bernhard, A. P., "Smart Helicopter Rotor with Active Blade Tips," Ph.D. Dissertation, Aerospace Engineering Dept., Univ. of Maryland, College Park, MD, Feb. 2000.

[56]Bernhard, A. P., and Chopra, I., "Trailing Edge Flap Activated by a Piezo-induced Bending–Torsion Coupled Beam," *Journal of the American Helicopter Society*, Vol. 44, No. 1, 1999, pp. 3–15.

[57]Bernhard, A. P., and Chopra, I., "A Bending–Torsion Coupled Actuator for a Smart Rotor with Active Blade Tips," *Smart Materials and Structures*, Vol. 10, No. 1, 2001, pp. 35–52.

[58]Bernhard, A. P., and Chopra, I., "Hover Testing of Active Rotor Blade-Tips Using a Piezo-induced Bending–Torsion Coupled Beam," *Journal of Intelligent Material Systems and Structures*, Vol. 9, No. 12, 1998, pp. 963–974.

[59]Chandra, R., and Chopra, I., "Structural Modeling of Composite Beams with Induced Strain Actuators," *AIAA Journal*, Vol. 31, No. 9, 1993, pp. 1692–1701.

[60]Bernhard, A. P., and Chopra, I., "Mach-Scale Design of a Rotor-Model with Active Blade Tips," *American Helicopter Society 55th Annual Forum*, Montreal, Canada, 1999, pp. 579–598.

[61]Sirohi, J., and Chopra, I., "Investigations on Piezoceramic Actuator Response," *SPIE's 5th Symposium on Smart Structures and Materials, Conference on Smart Structures and Integrated Systems*, Vol. 3329, edited by M. E. Regelbrugge, Society of Photo-Optical Instrumentation Engineers, Bellingham, WA, 1998, pp. 626–646.